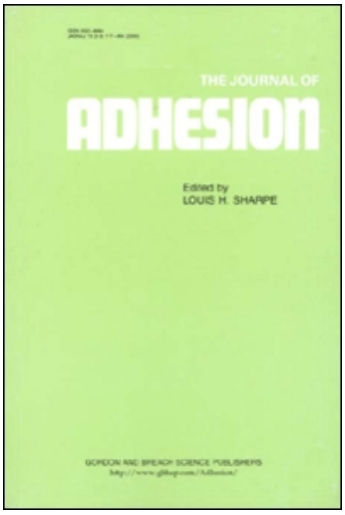

The Journal of Adhesion
Publication details, including instructions for authors and subscription information:
http://www.informaworld.com/smpp/title~content=t713453635

Load Ratio Effect on the Fatigue Behaviour of Adhesively Bonded Joints: An Enhanced Damage Model

K. B. Katnam[a]; A. D. Crocombe[a]; H. Khoramishad[a]; I. A. Ashcroft[b]
[a] Mechanical, Medical and Aerospace Engineering, University of Surrey, Guildford, Surrey, UK [b] The Wolfson School of Mechanical and Manufacturing Engineering, Loughborough University, Leicestershire, UK

Online publication date: 12 March 2010

To cite this Article Katnam, K. B. , Crocombe, A. D. , Khoramishad, H. and Ashcroft, I. A.(2010) 'Load Ratio Effect on the Fatigue Behaviour of Adhesively Bonded Joints: An Enhanced Damage Model', The Journal of Adhesion, 86: 3, 257 — 272
To link to this Article: DOI: 10.1080/00218460903462632
URL: http://dx.doi.org/10.1080/00218460903462632

The Journal of Adhesion, 86:257–272, 2010

ISSN: 0021-8464 print/1545-5823 online
DOI: 10.1080/00218460903462632

Taylor & Francis
Taylor & Francis Group

Load Ratio Effect on the Fatigue Behaviour of Adhesively Bonded Joints: An Enhanced Damage Model

K. B. Katnam[1], A. D. Crocombe[1], H. Khoramishad[1], and I. A. Ashcroft[2]
[1]Mechanical, Medical and Aerospace Engineering, University of Surrey, Guildford, Surrey, UK
[2]The Wolfson School of Mechanical and Manufacturing Engineering, Loughborough University, Leicestershire, UK

Structural adhesives are used widely in aerospace and automotive applications. However, fatigue damage in these adhesives is an important factor to be considered in the design of adhesively bonded structural members that are subjected to cyclic loading conditions during their service life. Fatigue life of adhesively bonded joints depends mainly on the fatigue load and the load ratio. A fatigue damage model is presented in this paper to include the effect of fatigue mean stresses on the failure behaviour of adhesively bonded joints. The fatigue damage model is developed using an effective strain-based approach. The model is implemented on a tapered single lap joint configuration and is validated by experimental test results. The adhesive layer in the tapered single lap joint is modelled by using a cohesive zone with a bi-linear traction-separation response. The adverse effect of increasing fatigue mean stresses on the failure behaviour of adhesively bonded joints is successfully predicted.

Keywords: Cohesive zone approach; Fatigue damage model; Mean stress effect; Structural adhesives; Tapered single lap joint; Traction-separation response

1. INTRODUCTION

The driving force behind the usage of advanced structural adhesives in the aerospace and automotive industries is to attain a low cost and light-weight design. However, an optimal structural design with more economical safety factors cannot be achieved without a comprehensive

Received 22 May 2009; in final form 11 September 2009.
Address correspondence to A. D. Crocombe, Mechanical, Medical and Aerospace Engineering, University of Surrey, Guildford, Surrey GU2 7XH, UK. E-mail: a.crocombe@surrey.ac.uk

understanding of the failure behaviour of these structural adhesives under different service conditions and without reliable lifetime predictive models. The design of adhesive joints in an adhesively bonded structure will be governed by different failure criteria such as ultimate strength, fatigue endurance, impact toughness, durability, etc. [1]. As cyclic loading conditions are common in aerospace and automotive structures, the fatigue behaviour of structural adhesives is important from a design viewpoint [2].

It is well known that the fatigue failure of structural adhesives depends on the mean as well as the maximum fatigue loads. These two fatigue loading parameters are related through the fatigue load ratio, R, which is the ratio of minimum to maximum fatigue load. It is necessary to ensure that the adhesively bonded structural members will not fail as a result of accumulated fatigue damage during their expected service life. Generally, at an early design stage, constant amplitude fatigue experimental tests are performed on coupon-level adhesive joints and S-N curves may be obtained for different load ratio, R, values. However, it would be expensive to have fatigue data for all possible R values. Numerical models that are capable of predicting the influence of the R value on the fatigue failure behaviour can help the engineer to design effectively.

In an aircraft, with a large number of composite structures, different structural members will be loaded at different load ratio values [3]. The mean stress effect on fatigue life of metals has been extensively investigated [4–6]. However, studies on polymer materials for the mean stress effect on fatigue are comparatively few [7]. A number of workers tested a range of adhesively bonded joints with various adhesives under cyclic loading and found that a traditional S-N curve can be used to relate the fatigue life to the applied loads [8–11]. A fatigue endurance limit was found that often appeared to range between 15 and 35% of the quasi-static strength of the joint for a number of adhesives at room temperature. The mean load effect on the fatigue behaviour has been experimentally investigated and it was found that increasing the mean load has a deleterious effect on the fatigue life for a fixed fatigue load range [12]. Similarly, Underhill and DeQuesnay performed fatigue tests on adhesive joints (Al 2024-T3 substrates and FM73 adhesive) and found that fatigue life decreases as mean load increases for a fixed fatigue load range. Further, they observed no frequency dependent effects on fatigue life in the 10 to 60 Hz range [13]. Hysteritic heating was probably conducted away through the substrates and at these frequencies any creep effect will be minimised.

In this paper, a numerical model that accounts for the mean stress effect is developed to predict the fatigue behaviour of adhesively

bonded joints. An effective strain-based fatigue damage parameter is used for the adhesive material. The fatigue model is validated by experimental test data reported in [12].

2. MEAN STRESS EFFECT

Structural members subjected to in-service cyclic loads exhibit a fatigue behaviour that generally depends on the mean stress values. For a given fatigue load range a tensile mean normal stress has a detrimental effect on fatigue strength, whereas, in general, a compressive mean normal stress has a beneficial effect [14]. The problem of the mean stress effect on fatigue life has been approached practically by developing empirical relationships. For metals and alloys, various criteria have been proposed to deal with the mean stress effect on fatigue life, such as Soderberg, Goodman, and Gerber diagrams. The alternating stress amplitude, σ_a (half the stress range), *versus* the mean stress, σ_m, diagrams are used for the three criteria as shown in Fig. 1. The lines on this figure refer to combinations of alternating and mean stresses that have the same fatigue lives or endurance limit. Note that as the mean stress increases, the alternating stress that has the same life drops, as expected. The limiting maximum mean stress is chosen as either ultimate strength, σ_u, as in the Goodman and Gerber criteria, or the yield strength, σ_y, as in the Soderberg criterion. The alternating stress amplitude at zero mean stress is denoted as $\sigma_{\tilde{a}}$:

$$\text{Soderberg criteria}: \qquad \frac{\sigma_a}{\sigma_{\tilde{a}}} + \frac{\sigma_m}{\sigma_y} = 1 \tag{1}$$

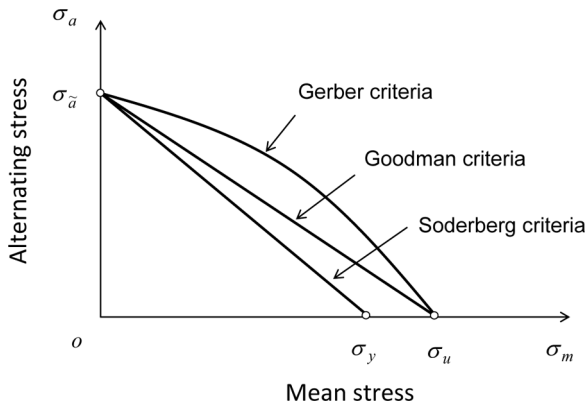

FIGURE 1 The mean stress effect on fatigue life: Soderberg, Goodman, and Gerber criteria.

$$\text{Goodman criteria}: \quad \frac{\sigma_a}{\sigma_{\tilde{a}}} + \frac{\sigma_m}{\sigma_u} = 1 \tag{2}$$

$$\text{Gerber criteria}: \quad \frac{\sigma_a}{\sigma_{\tilde{a}}} + \left(\frac{\sigma_m}{\sigma_u}\right)^2 = 1. \tag{3}$$

The curves are determined experimentally by obtaining a series of S-N curves for different load ratio values (varying the load ratio will result in varying the ratio of the mean to alternating stress components). In this paper, the Goodman criterion is adopted to predict the fatigue failure behaviour of adhesively bonded joints as the experimental work [12] indicated this was appropriate.

3. FATIGUE DAMAGE MODEL

The total fatigue life of adhesively bonded joints can be divided into two parts: a damage initiation phase (including coalescence) and a damage propagation phase. The contribution of the damage initiation phase to the total fatigue life increases with reduced fatigue stress levels. As fracture mechanics-based numerical approaches cannot be used to model the damage initiation and the damage propagation together, a damage mechanics approach is employed to model the fatigue damage in adhesive joints.

The fatigue damage accumulation at any given material point is assumed to occur as a result of increasing local strain with the number of fatigue cycles. By relating this increase in the local strain to a damage parameter, an effective strain-based fatigue damage model is developed. This is explained in Fig. 2. If an adhesive joint is subjected to a sinusoidal constant-amplitude fatigue loading as shown in Fig. 2a, the maximum principal strain, $\varepsilon_{p,\max}$, increases with time (or number of cycles) at any material point A in the adhesive layer and reaches the adhesive failure strain, ε_f, before the material fails at that point as shown in Fig. 2b. A damage parameter, D, can be defined such that $\varepsilon_{p,\max}$ reaches ε_f when it varies from 0 to 1, as shown in Fig. 2b. The fatigue damage parameter is considered to be a function, ψ, of the maximum principal fatigue strain, $\varepsilon_{p,\max}$, the number of fatigue cycles, N, and the load ratio, R, as in Eq. (4):

$$D = \psi(\varepsilon_{p,\max}, N, R). \tag{4}$$

By considering a two-parameter exponential form [15,16], the cyclic damage rate is modelled as:

$$\frac{\Delta D}{\Delta N} = \alpha(\varepsilon_{eff})^{\beta}. \tag{5}$$

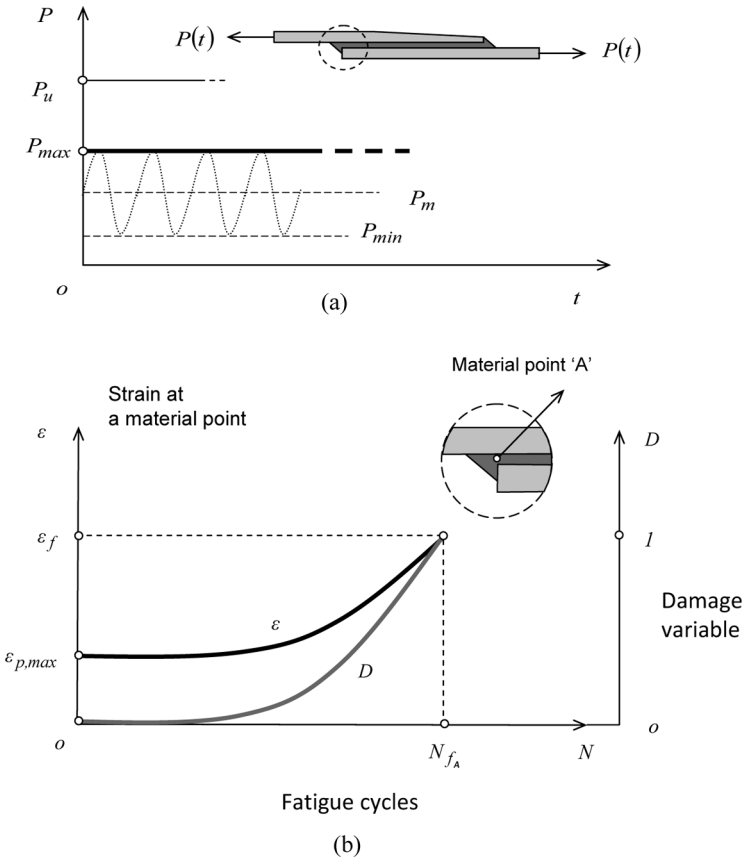

FIGURE 2 The fatigue damage model: (a) The constant amplitude fatigue loading and (b) the fatigue strain and damage accumulation.

In Eq. (5), $\varepsilon_{eff} = (\varepsilon_{p,\max} - \varepsilon_o)\lambda$, where ε_{eff} is the effective fatigue strain, λ is a correction factor for the mean stress effect and ε_o is the threshold strain (a strain below which fatigue damage does not occur). The constants α, β, and ε_o in Eq. 5 are material dependent and govern the fatigue damage evolution in an adhesive system. The threshold strain and the load ratio in the damage equation ensure a fatigue prediction that includes the fatigue endurance limit and the mean stress effect.

The correction factor, λ, which is a function of the load ratio, R, and the maximum fatigue load, $P_{\max}$, is derived from the assumption that the mean stress effect in the adhesive joint follows the Goodman empirical relationship. A Goodman diagram for a constant fatigue life is shown in Fig. 3. For a given adhesive joint, the points $A(\sigma_{m1}, \sigma_{a1})$

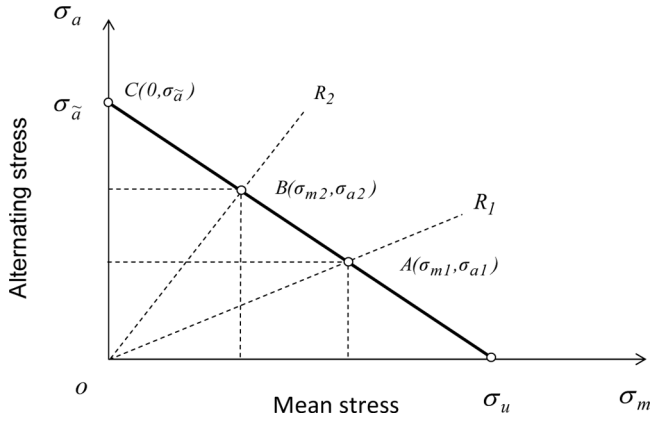

FIGURE 3 The Goodman constant fatigue life diagram.

for R_1 and $B(\sigma_{m2}, \sigma_{a2})$ for R_2 have the same fatigue life. However, the maximum fatigue stress at A, $\sigma_{\max 1} = \sigma_{m1} + \sigma_{a1}$, and at B, $\sigma_{\max 2} = \sigma_{m2} + \sigma_{a2}$, can be related to the maximum fatigue stress at C, which is $\sigma_{\tilde{a}}$, by the correction factor, λ, as in Eq. (6):

$$\sigma_{\tilde{a}} = \lambda(\sigma_{\max 1}, R_1)\sigma_{\max 1} = \lambda(\sigma_{\max 2}, R_2)\sigma_{\max 2}. \tag{6}$$

Further, by substituting $\sigma_m = (1+R)\sigma_{\max}/2$ and $\sigma_a = (1-R)\sigma_{\max}/2$ in the Goodman relationship [Eq. (2)] and rearranging the equation for $\sigma_{\tilde{a}}$ gives:

$$\sigma_{\tilde{a}} = \frac{(1-R)\sigma_{\max}}{\left[2 - \frac{\sigma_{\max}(1+R)}{\sigma_u}\right]} = \lambda(\sigma_{\max}, R)\sigma_{\max}. \tag{7}$$

In Eq. (7) the correction factor, λ, which is a function of $\sigma_{\max}$ and R, is:

$$\lambda(\sigma_{\max}, R) = \frac{1-R}{\left[2 - \frac{\sigma_{\max}(1+R)}{\sigma_u}\right]}. \tag{8}$$

It can be seen from Eq. (8) that the value of the correction factor, λ, varies from 0 to 1 as the load ratio varies from 1 to -1. Further, the correction factor given in Eq. (8) is employed for the current fatigue model and the results are discussed in Section 6.

4. EXPERIMENTAL TESTS

The fatigue tests performed by Crocombe and Richardson [12] on a tapered single lap joint (TSLJ) configuration, see Fig. 4, for different

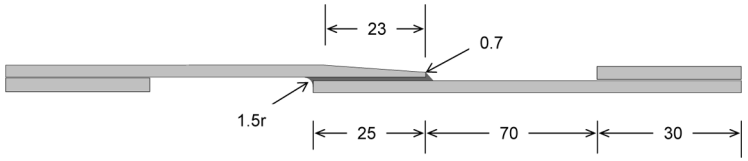

FIGURE 4 The geometric configuration of the tapered single lap joint (specimen width = 12.5 mm; adhesive thickness = 0.165 mm; substrate thickness = 3.6 mm).

load ratio values revealed that, for a given stress range, increasing the mean stress has a deleterious effect on the fatigue life. The experimental fatigue data that were reported in [12] have been used to validate the fatigue damage model presented in the current paper.

The adhesive used in the study was AV119, a hot cure, rubber toughened epoxy, from Huntsman Ltd., Duxford, UK. The substrate material was steel. Material tests were carried out on the substrate material and values for yield and ultimate stresses were found to be 500 and 650 MPa, respectively. The average quasi-static joint failure load was observed to be 13.7 kN. Full failure fatigue tests were carried out at three different load ratios ($R = 0.1$, 0.5, and 0.75). Fatigue damage initiated in the adhesive fillet near the free end of the full thickness substrate and travelled across the adhesive layer and then adjacent to the loaded substrate interface.

5. FINITE ELEMENT MODELLING

The cohesive zone model (CZM) has been employed for a wide variety of problems, and materials including metals, ceramics, polymers, and composites. The CZM was developed in a continuum damage mechanics framework and made use of fracture mechanics concepts to improve its applicability. The CZM was originally introduced by Barenblatt [17] based on the Griffith's theory of fracture and Dugdale [18] extended the approach to perfectly plastic materials. Other researchers [19–21] then extended the CZM model by proposing various traction-separation functions and applying it to different problems.

The current fatigue damage model is implemented using cohesive zone elements in Abaqus/Standard version 6.7 (Dassault Systèmes, Simulia, Warrington, UK). The adhesive layer in the TSLJ is modelled by employing two-dimensional cohesive zone elements (COH2D) with a bi-linear traction-separation response. The concept of cohesive fracture and traction-separation response is schematically illustrated in Fig. 5. When the adherends are loaded, cracks nucleate in a small

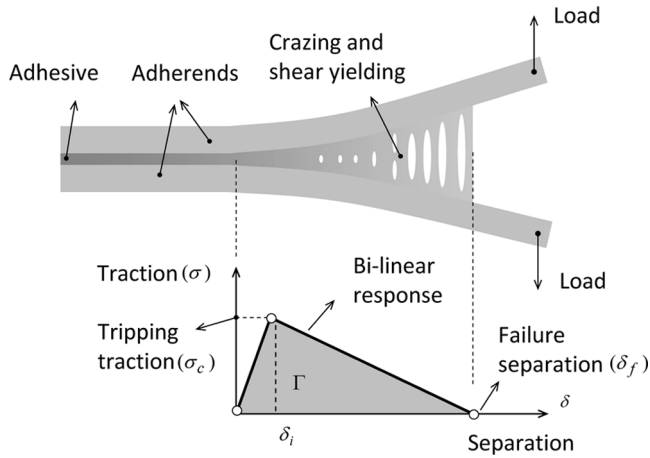

FIGURE 5 The schematic of traction-separation response in a cohesive zone.

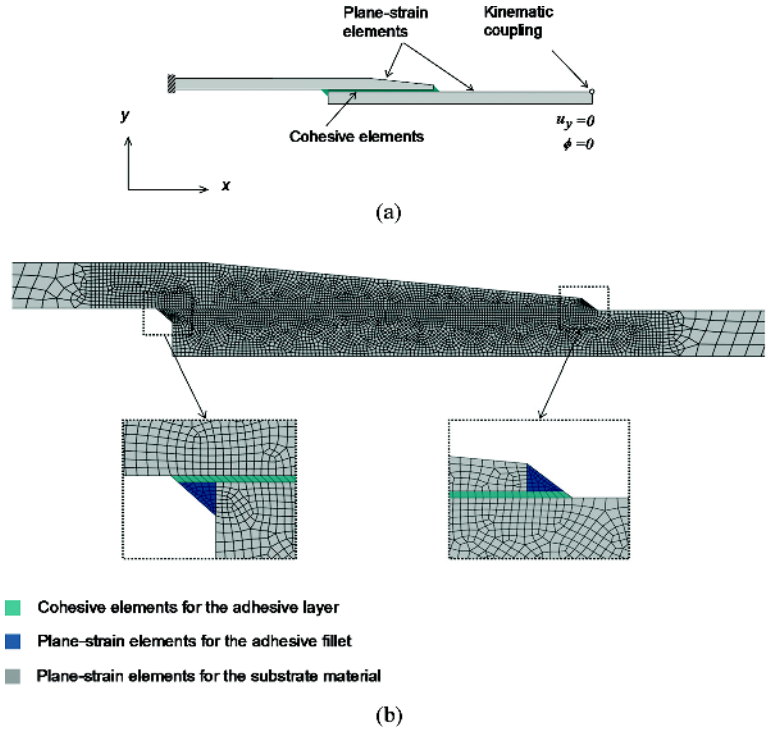

FIGURE 6 The cohesive zone modelling of the TSLJ: (a) the boundary conditions and (b) the finite element types assigned to the tapered single lap joint.

fracture process zone due to crazing and shear yielding of the adhesive. In this process zone, adhesive stress (traction) initially increases with separation and starts to decrease after reaching a maximum value (tripping traction). The adhesive stresses reach zero when the separation reaches a certain value (δ_f, failure separation). A bi-linear traction-separation response (see Fig. 5) is assumed in the current model—though different response curves (*e.g.*, trapezoid) have been employed to model cohesive zones [20]. The area of the triangle represents the fracture energy (Γ) of the adhesive. Further, a mixed-mode analysis can be performed by defining traction-separation responses for peel and shear. The boundary conditions and the finite element types assigned to the TSLJ are shown in Fig. 6. The left-side boundary is fixed, and the vertical deflection and the rotation at the right-side boundary are constrained by kinematically coupling the nodes. The substrate material is modelled with plane-strain elements (CE4). As a sweep mesh is required to define the peel direction for the cohesive zone in Abaqus, the fillet region is divided into a cohesive and a fracture-free zone as shown in Fig. 6. A material and geometrical non-linear analysis is performed. The cohesive zone element size is between 0.165×0.165 and 0.2×0.165 mm.

6. RESULTS AND DISCUSSIONS

The cohesive zone model is implemented to predict the static strength and the fatigue failure behaviour of the TSLJ. The static response of the TSLJ is validated and the cohesive zone parameters are determined using the experimental test data.

6.1. The Static Failure Analysis

A non-linear static analysis is performed for the TSLJ using the cohesive zone elements. A mixed-mode damage criterion available in Abaqus/Standard, the Benzeggagh-Kenane law [22], is used in the analysis to include the effect of mode-mixity on the static failure behaviour. In order to use a traction-separation response, the fracture energies, (Γ_I, Γ_{II}), and the tripping tractions, (σ_c, τ_c), for peel and shear are required. The fracture energy of the adhesive AV119 for Mode I was obtained from experimental test data [11,24]. As the fracture energy of adhesives depend on the bondline thickness, an extrapolated fracture energy value, $\Gamma_I = 1.2\,\text{kJ/m}^2$, is obtained for 0.165 mm adhesive thickness from the experimental test data available for Mode I failure. The fracture energy for shear, Γ_{II}, is assumed as $2.4\,\text{kJ/m}^2$ (twice the value of Mode I fracture energy). The Young's modulus,

E, and the Poisson's ratio, ν, of AV119 adhesive are 2800 MPa and 0.4, respectively [24].

A series of static failure analyses are conducted for different tripping traction values and the static failure loads are predicted. This is shown in Fig. 7. The effect of the tripping traction value on the static failure load divided the tripping traction range into three regions (Zone A, B, and C), as mentioned in Liljedahl *et al.* [25]. The three Zones A, B, and C in Fig. 7 represent the effect of tripping traction on the static failure strength for a fixed fracture energy value. The size of the fracture process zone depends on the tripping traction and the fracture energy values. However, for a given fracture energy, the size of the process zone will be decreased with increasing tripping traction values and *vice versa*. In a finite element model, if the size of the process zone is less than the length of the cohesive elements used to model the adhesive layer, *i.e.*, Zone C, the solution will be highly mesh-dependent. Moreover, if the tripping traction value is very low, *i.e.*, Zone A, a large process zone will exist in the model—these two scenarios should generally be avoided. In Zones A and C (see Fig. 7), the failure load is more dependent on the tripping traction. However, the failure load is found to be less dependent on the tripping traction values in Zone B. Zone C involves a discontinuous process zone which is a result of insufficient mesh size and should be avoided. As the average static failure load obtained from the experimental tests was

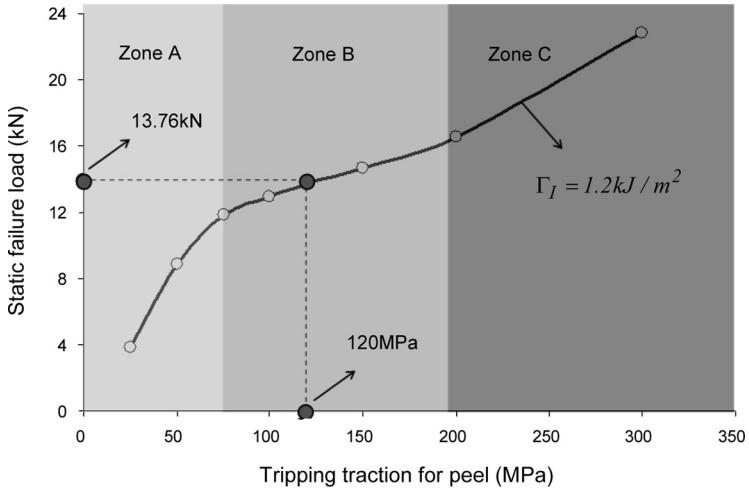

FIGURE 7 The variation of the static failure load predicted for different tripping tractions.

13.7 kN for the TSLJ; the corresponding tripping traction values are calculated for Fig. 7. The tripping tractions values obtained are $\sigma_c = 120\,\text{MPa}$ and $\tau_c = 70\,\text{MPa}$ for peel and shear, respectively. By using the set of cohesive parameters, (Γ_I, Γ_{II}, σ_c, τ_c) = (1.2,2.4,120, 70), the static failure analysis is performed and a static strength of 13.76 kN is predicted, which is less than 1% variation from the average static failure obtained from the experimental tests. The damage predicted from the static model initiates from the adhesive fillet adjacent to the free end of the full thickness substrate, which is in agreement with the experiments [12].

6.2. The Fatigue Failure Analysis

A fatigue failure analysis is performed on the TSLJ using the damage equation [Eqs. (5) and (8)] derived in Section 3 to predict the fatigue failure behaviour. In the current fatigue model the sinusoidal fatigue loading is represented by a constant loading equal to the maximum load level in actual cyclic loading. The fatigue damage is modelled by degrading the bi-linear traction-separation response and is implemented by using a user-subroutine (USDFLD) in Abaqus/Standard. The cohesive zone model parameters have been set to decrease linearly with the damage parameter. The user-subroutine USDFLD redefines field variables at element integration points and, thus, allows defining solution-dependent material properties. Initially, the maximum principal strains induced by the maximum fatigue load in the adhesive layer were calculated using a static analysis. These maximum principal strains were then used to calculate the cyclic fatigue damage rate based on Eq. (5). The material properties of the adhesive layer were degraded based on the fatigue damage parameter using USDFLD user-subroutine. The traction-separation response of the adhesive material was defined as solution-dependent by degrading the fracture energies and the tripping tractions based on the calculated fatigue damage parameter. Each increment in the analysis represented a block of fatigue cycles and the traction separation response was degraded at each material point each increment. The increments continued until the joint failed, thus indicating the fatigue life of the joint. The implementation of this procedure is explained in detail in Khoramishad *et al.* [16]. The set of cohesive parameters, (Γ_I, Γ_{II}, σ_c, τ_c) = (1.2,2.4,120,70), which are used for the static failure prediction, is employed in the fatigue analysis and these are degraded to zero as the damage at a point increases from 0 to 1. By applying the maximum fatigue load, $P_{\max}$ (see Fig. 2a), the initial stresses in the adhesive are predicted. Further, the solution-dependent field variable is calculated using

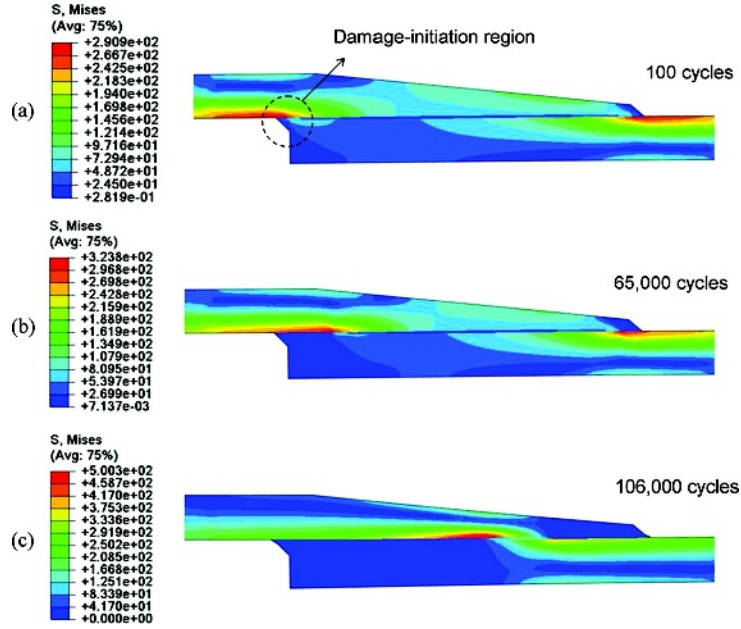

FIGURE 8 The von Mises stress distribution in the TSLJ after N = 100, N = 65,000, N = 106,000 for R = 0.1 and $(P_{\max} - P_{\min})/P_u = 0.27$.

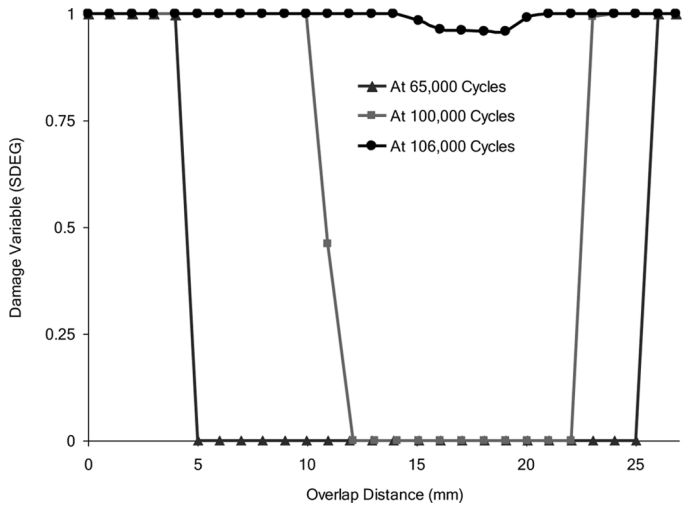

FIGURE 9 The damage distribution in the adhesive layer along the overlap in the TSLJ after N = 65,000, N = 100,000 and N = 106,000 for R = 0.1 and $(P_{\max} - P_{\min})/P_u = 0.27$.

the user-subroutine USDFLD at every increment and the cohesive material properties are degraded and updated for the next increment.

A parametric study is conducted to predict the fatigue failure life of the TSLJ for different damage parameters (α, β, ε_0) in Eq. (5) for the load ratio $R = 0.1$. The predicted S-N curves are validated against the experimental data reported by Crocombe and Richardson [12] for $R = 0.1$ and a good correlation is attained for (α, β, ε_o) = (16,2,0.02), see Fig. 11 later. These values were achieved by manual iteration. The predicted fatigue damage initiation and propagation are shown in Fig. 8. The von Mises stress distribution indicates that stress concentrations exist near the fillet regions, with the fillet adjacent to the stiffer unloaded substrate being critical to initiate fatigue damage (see Fig. 8a, after 100 fatigue cycles). After damage has initiated near the embedded substrate corner, the predicted fatigue crack propagated from both the fillets into the middle of the joint as shown in Figs. 8b and 8c after 65,000 and 106,000 cycles. The predicted fatigue

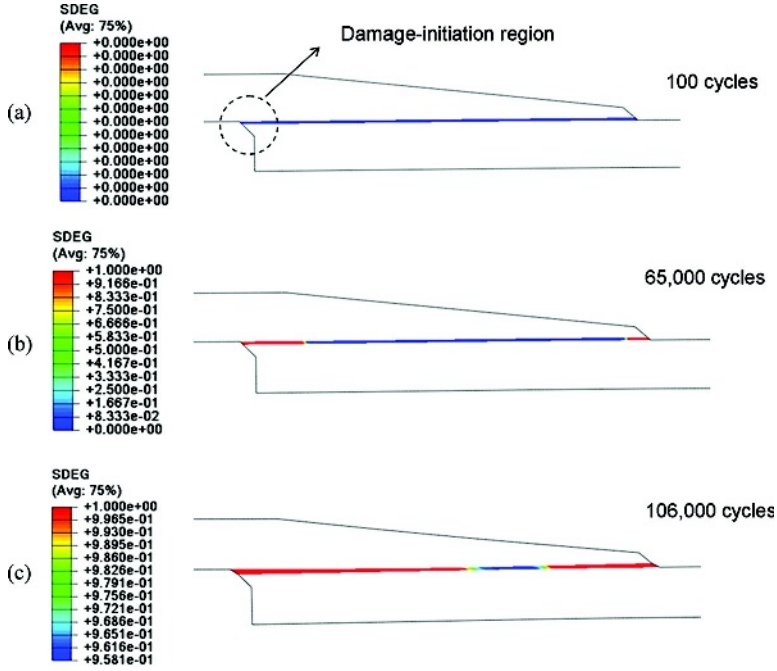

FIGURE 10 The damage distribution in the adhesive layer along the overlap in the TSLJ after N = 100, N = 65,000, N = 106,000 for R = 0.1 and $(P_{\max} - P_{\min})/P_u = 0.27$.

life is 106,000 cycles for $R = 0.1$ and $(P_{\max} - P_{\min})/P_u = 0.27$ (the data point encircled in Fig. 11).

The variation of the damage variable (SDEG in Abaqus/Standard) with the overlap length at different fatigue cycles is shown in Fig. 9. The transitions from SDEG = 0 to SDEG = 1 in the plots represent the length of the cohesive process zone. The variation of the slope of the transition region with the number of fatigue cycles indicates that the length of the process zone increases as the crack tip moves towards the middle of the joint. This causes a sudden failure of the joint after a certain crack length as the maximum applied fatigue load can no longer be sustained. Further, contour plots of the damage distribution in the TSLJ is shown in Fig. 10 after N = 100, N = 65,000, and N = 106,000 cycles. This process is repeated at three other load levels and the excellent fit to the experimental fatigue life data can be seen in Fig. 11.

These same damage parameters, $(\alpha,\ \beta,\ \varepsilon_o) = (16,2,0.02)$, are then employed to predict the fatigue failure behaviour of the TSLJ at different load ratios and load levels. Three load levels for $R = 0.5$ and two load levels for $R = 0.75$, corresponding to the experimental data [12], are analysed and the S-N curves (the normalised load range *versus* fatigue cycles) are predicted. The predicted results are then compared with the experimental test data and are found to be in good agreement as shown in Fig. 11, thus validating the calibrated fatigue damage parameters.

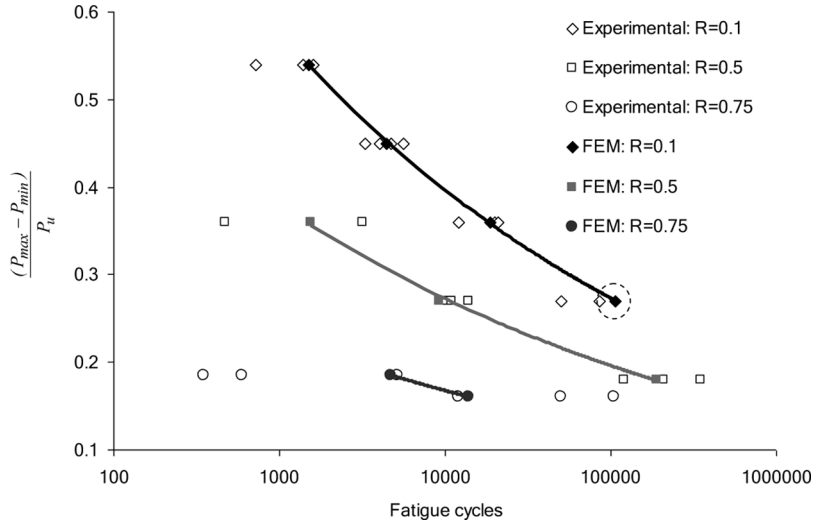

FIGURE 11 Validation of the fatigue damage model: The load-life curves (the normalised load range versus fatigue cycles) for R = 0.1, R = 0.5 and R = 0.75.

7. CONCLUSIONS

A fatigue damage model is developed to include the effect of mean stresses on the fatigue life predictions in adhesively bonded joints. An effective strain-based damage parameter is used to degrade the adhesive material under cyclic stresses. The damage parameter is a function of four fatigue variables: the maximum principal strain, fatigue cycles, fatigue threshold strain and the load ratio. The Goodman empirical relationship is employed to define a correction function to calculate an effective fatigue strain, and to predict the fatigue damage in the adhesive material. A tapered single lap joint configuration (steel substrates and AV119 adhesive [12]) is used to validate the fatigue damage model. A cohesive zone approach is employed for the adhesive material with a bi-linear traction-separation response. The cohesive parameters are degraded based on a solution-dependent user-defined field in Abaqus/Standard and the fatigue failure behaviour is predicted for different load levels and load ratios. The predicted fatigue results are compared with the experimental test data and a good correlation is found.

REFERENCES

[1] Higgins, A., *Int. J. Adhes. Adhes.* **20**, 367–376 (2000).
[2] Goranson, U. G., *Int. J. Fatigue* **20** (6), 413–431 (1997).
[3] Schon, J., *Compos. Sci. Technol.* **61**, 1143–1149 (2001).
[4] Fang, D. and Berkovits, A., *Int. J. Fatigue* **16** (6), 429–437 (1994).
[5] Koh, S. K., Oh, S. J., Li, C., and Ellyin, F., *Int. J. Fatigue* **21** (10), 1019–32 (1999).
[6] Strizak, J. P. and Mansur, L. K., *J. Nucl. Mater.* **318**, 151–156 (2003).
[7] Tao, G. and Xia, Z., *Int. J. Fatigue* **29**, 2180–2190 (2007).
[8] Smith, M. A. and Hardy, R., Fatigue research on bonded carbon fibre-composite metal joints. RAE Tech. Rep. 77072 (Royal Aircraft Establishment, Farnborough, 1977).
[9] Harris, J. A. and Fay, P. A., *Int. J. Adhes. Adhes.* **12** (1), 9–18 (1992).
[10] Mays, G. C., Fatigue and creep performance of epoxy resin adhesive joints. Transport and road research laboratory, Contractor Report 224 (Transport and Road Research Laboratory, Crowthorne, 1990).
[11] Crocombe, A. D., Fatigue failure of AV119 and F241 strap lap shear joints, MTS Adhesives Project 2 (DTI). Report 6: Annex 6 (AEA Technology, Harwell, Didcot, 1996).
[12] Crocombe, A. D. and Richardson, G., *Int. J. Adhes. Adhes.* **19**, 19–27 (1999).
[13] Underhill, P. R. and DeQuesnay, D. L., *Int. J. Adhes. Adhes.* **26**, 62–66 (2006).
[14] Susmel, L., Tovo, R., and Lazzarin, P., *Int. J. Fatigue* **27**, 928–943 (2005).
[15] Graner Solana, A., Crocombe, A. D., and Ashcroft, I. A., *Int. J. Adhes. Adhes.* (2009) (submitted).
[16] Khoramishad, H., Crocombe, A. D., Katnam, K. B., and Ashcroft, I. A., *Int. J. Fatigue* (2009) (submitted).
[17] Barenblatt, G. I., *Advan. Appl. Mech.* **7**, 55–129 (1962).

[18] Dugdale, D. S., *J. Appl. Mech.* **8**, 100–104 (1960).
[19] Alfano, G., *Compos. Sci. Technol.* **66** (6), 723–730 (2006).
[20] Diehl, T., *Int. J. Adhes. Adhes.* **28** (4–5), 237–255 (2008).
[21] Diehl, T., *Int. J. Adhes. Adhes.* **28** (4–5), 256–265 (2008).
[22] Benzeggagh, M. L. and Kenane, M., *Compos. Sci. Technol.* **56**, 439–449 (1996).
[23] Lee, R. J., Butler, J. R., Yates, T., and Davidson, R. Test Methods for Adhesive Fracture Properties, MTS Adhesives Project 2, Report 5: Annex 1 (AEA Technology, Harwell, Didcot, 1997).
[24] Loh, W. K., Crocombe, A. D., Abdel Wahab, M. M., and Ashcroft, I. A., *Eng. Fract. Mechs.* **69**, 2113–2128 (2002).
[25] Liljedahl, C. D. M., Crocombe, A. D., Wahab, M. A., and Ashcroft, I. A., *Int. J. Fracture* **141** (1–2), 147–161 (2006).